Evaluation of cyclic loading effects on residual stress relaxation in offshore wind welded structures

Article *in* Journal of Multiscale Modelling · June 2021

DOI: 10.1142/S1756973721500050

CITATIONS
0

READS
230

4 authors:

Giuseppe Statti
Cranfield University
1 PUBLICATION **0** CITATIONS
SEE PROFILE

Ali Mehmanparast
Cranfield University
95 PUBLICATIONS **688** CITATIONS
SEE PROFILE

Romali Biswal
Cranfield University
10 PUBLICATIONS **104** CITATIONS
SEE PROFILE

Cesare Mario Rizzo
Università degli Studi di Genova
99 PUBLICATIONS **496** CITATIONS
SEE PROFILE

Evaluation of cyclic loading effects on residual stress relaxation in offshore wind welded structures

Giuseppe Statti[1], Ali Mehmanparast[1*], Romali Biswal[2], Cesare Mario Rizzo[3]

[1] Offshore Renewable Energy Engineering Centre, Cranfield University, Cranfield, UK

[2]Welding Engineering and Laser Processing Centre, Cranfield University, Cranfield, UK

[3]University of Genoa, DITEN, Via Montallegro 1, Genova 16145, Italy

Corresponding author: a.mehmanparast@cranfield.ac.uk

Abstract

Monopile foundations contain welding residual stresses and are widely used in industry to support offshore wind turbines. The monopiles are subjected to hammering loads during installation and cyclic loads during operation, therefore the influence of residual stress redistribution as a result of fatigue cycles must be evaluated in these structures. The existing empirical models to predict the residual stress redistribution in the presence of cyclic loading conditions are strongly dependent on the material, welding process and loading conditions. Hence, there is a need to predict the residual stress redistribution using finite element simulations. In this study numerical analyses have been conducted to predict the initial state of residual stress in a simplified weld geometry and examine the influence of subsequent cyclic loads on the relaxation behaviour in residual stress profiles. The results have shown that fatigue cycles have a severe effect on residual stress relaxation with the greatest reduction in residual stress values observed in the first cycle. Moreover, the numerical prediction results have shown that the stress amplitude plays a key role in the extent of residual stress relaxation in welded structures.

1 Introduction

Since the Industrial Revolution, the energy need in the world has dramatically increased with the fossil fuel resources playing a key role to satisfy the energy demand around the world. Nowadays the fossil fuels still contribute to approximately three-quarters of the energy consumption in the European Union [1]. However, the evolving awareness around the harmful effects of fossil fuels on CO_2 emissions and global warming has led to more interest towards sustainable sources of clean energy. Among various sources of renewable energy, wind power is recognised as one of the most efficient and accessible sources of energy to realise the short- and long-term energy demands particularly in Europe, which has rich sources of onshore and offshore wind energy. While onshore wind is known to be a well-established industry with thousands of wind farms operating around the world since the last few decades, more investments have been made in recent years to bring down the cost of electricity generation from offshore wind energy and make it more competitive with alternative sources of energy. Due to the decreasing trend in the Levelised Cost of Energy (LCoE) the installed offshore wind capacity has significantly increased in recent years. This has resulted in 22 GW of installed offshore wind capacity in Europe in 2019, from over 5000 grid-connected offshore wind turbines across 12 countries [2]. Following the increasing trend in the number of offshore wind turbine (OWT) installations in Europe, the design and structural integrity assessment of these structures has become an important topic to achieve improved asset integrity management plans for the current and future installations. Particularly, it is known that the current designs for the OWT support structures are conservative in order to ensure that the OWTs can safely complete the

operational lifespan that they have been designed for. Therefore, the design and life assessment of future generation of OWT support structures must be enhanced to further reduce the LCoE of offshore wind power.

The type of fixed-bottom OWT support structure depends on the water depth and the distance from the shore, with the monopile foundations being the preferred support structures for relatively shallow waters whereas jacket structures are considered for deployment of OWTs in deeper waters. The total number of installed OWTs supported using various types of foundations at the end of 2019 in Europe are shown in Figure 1. As seen in this figure, over 80% of OWTs are supported by fixed-bottom monopile foundations [2], [3]. Monopiles are installed in shallow waters, with the depth of up to 50 m. They are made of structural steel plates which are firstly cold-formed and then multi-pass butt-welded in longitudinal and circumferential directions [4]. OWT monopiles have diameters varying between 3 and 10 m and wall thicknesses ranging between 40 and 150 mm [5], [6]. These support structures are subject to cyclic loading conditions in the harsh offshore environments, due to the presence of wind, wave and current forces, which act horizontally on the support structures. In addition, the foundations are subject to the vertical cyclic loads from other components of the structure such as the transition piece, tower and rotating blades. The cyclic loading condition in conjunction to the corrosion damage, which arises from the direct contact of the OWT foundations with seawater, introduces both fatigue and corrosion damage in these metallic structures. Therefore, corrosion-damage is known as the dominant failure mechanism in OWT support structures, particularly at the circumferential weld sections of monopiles which are the critical parts of the structure with higher likelihood of crack initiation and propagation due to the complexity of microstructures and locked-in residual stresses [4], [7], [8].

An important issue which influences the fatigue and corrosion-fatigue damage initiation and evolution in welded structures, is the residual stress profile which is introduced into the structure during the fabrication process. These locked-in stresses can cause a significant amount of uncertainty in the evaluation of the remaining life of welded structures if they are not properly measured and considered in the life assessment procedures. More importantly, even if residual stresses are quantified and mapped at the beginning of the operation, they might change during the lifespan due to the exertion of various static and cyclic loading conditions on the welded structures.

The purpose of the present study is to comprehensively investigate the influence of cyclic loading conditions on the residual stress redistribution in welded structures by reviewing the existing data in the literature. Subsequently, the collated data will be further analysed and interpreted to understand the significance of cyclic loading effects on residual stress redistribution in OWT monopile weldments. Moreover, finite element simulations have been performed to predict the residual stress relaxation under different loading conditions. As a matter of fact, this study aims to develop a deep understanding of the beneficial or damaging effects of residual stress redistribution and relaxation which may occur during both installation and operation phases. The results from this study are discussed in terms of the importance of residual stresses in the life assessment of offshore wind structures and the required direction for future research to enhance the structural design and life assessment of current and future generation of offshore wind monopiles.

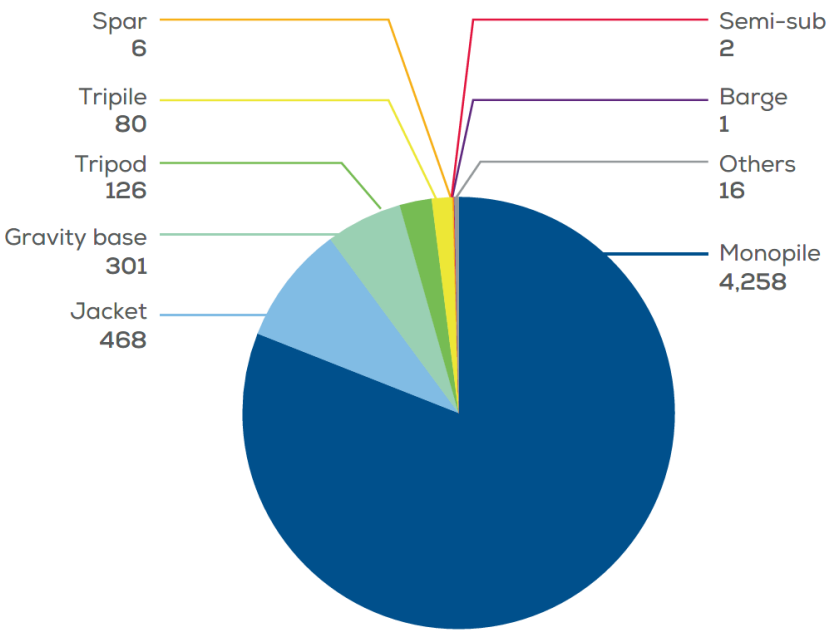

Figure 1: The number of installed OWTs supported using various types of foundations at the end of 2019 [2]

2 Residual stress relaxation mechanisms

In order to develop an understanding of the residual stress behaviour under different loading conditions, the physical and structural mechanisms related to the relaxation of residual stresses are reviewed and discussed in this section. The comparison of the findings from different studies provides a state-of-the-art on the residual stress redistribution in components and structures employed in a range of engineering applications. It is worth noting that the mechanisms reviewed and discussed below only describe the residual stress relaxation under cyclic loads to better understand the structural integrity of offshore structures, which are subjected to variable amplitude loading conditions. Therefore, the effects of other contributing factors such as time-dependent creep deformation (for high temperature components) and environmental damage (such as pitting corrosion) are not reviewed as they are beyond the scope of the present study.

Morrow and Sinclair [9] investigated the stress redistribution under cyclic loading conditions and reported that the principal cause of stress relaxation can be attributed to the accumulation of plastic strains during cyclic loading. They have suggested that the influence of residual stress on fatigue life assessment of components and structures can be evaluated by considering the change in the mean stress as a result of the locked-in stresses. Moreover, Morrow and Sinclair stated that the redistribution of residual stress is primarily dependent on the hardness of the material. Therefore, for a hard material with a greater yield stress, the residual stresses are less likely to relax under cyclic loading conditions whereas in soft materials, higher level of relaxation is expected to happen due to the accumulation of plastic strains in materials with lower yield stress.

Another study to understand the residual stress relaxation mechanism was carried out by James [10] who described residual stress redistribution under cyclic loading conditions based on the following criteria:

i. **Stresses above the macroscopic yield strength:** According to the findings from James' study, when the effective stress at the net section or the outer surface of an engineering component exceeds the nominal yield strength of the material, the resulting widespread plasticity leads to

full redistribution of residual stresses. Although engineering structures are often designed for operation below the yield strength of the material, plastic deformations would start to occur when an overload happens due to extreme operational loading conditions or when notches and defects start to form, acting as stress risers in the structure. Moreover, upon formation of macro-level plasticity at the outer surface of the structure, when the applied load is removed, the induced residual stress will act in the opposite direction, compared to the loading axis, due to the elastic-plastic material deformation mismatch in the subsurface layers. This means that, if the outer surface is plastically deformed under compression, the resulting residual stresses will be in tension and vice versa [10].

ii. **Stresses below the fatigue endurance limit:** Based on the observations conducted by James, when the structure is subjected to cyclic stresses below the fatigue endurance limit of the material, the redistribution of residual stresses may occur only at the later stages in fatigue life and it is highly likely that the low-stress residual stress relaxation mechanism would be completely different compared to that of observed at high-stress amplitudes [10].

iii. **Stresses between the macroscopic yield strength and the fatigue endurance limit:** Most engineering structures are designed for operational loading conditions between the fatigue endurance limit and the macro-level yield stress of the material. It is important to underline that, even if the macroscopic yielding does not occur in this regime, a localised yielding can occur at the outer surface of the structure. According to James [10], the redistribution of residual stresses under intermediate cyclic load levels is mainly found in the first few cycles and the relaxation behaviour would gradually diminish as the number of fatigue cycles increase. In addition, James [10] suggested that the residual stress relaxation under intermediate cyclic load levels continues to occur until it reaches an asymptotic non-zero value.

It is important to note that, while the criteria given above can describe the residual stress relaxation behaviour under uniform cyclic loading conditions, the offshore structures are subjected to variable amplitude cyclic loading conditions. In other words, the welded joints in OWT monopile can experience stress levels beyond the yield strength, below the fatigue endurance limit and intermediate stress levels falling in between these two. This means that a combination of different residual stress relaxation regimes would be needed to account for the structural integrity assessment of offshore structures such as OWT monopiles, experiencing stochastic loading conditions during their service life [11]–[13]. Moreover, assuming that the initial mean stress in the presence of residual stress is above the yield strength in a structure at the beginning of the operation, according to the first criterion described by James [10], the widespread plasticity can drop the residual stress to somewhere between the yield strength and fatigue endurance limit (second criterion) with the possibility of further residual stress relaxation to a stress level below the endurance limit (third criterion) after a few extra cycles [14].

Another contribution to the general understanding of the residual stress relaxation mechanisms was made by Hensel et al. [15], where the residual stresses were analysed with the hypothesis that the relaxation occurs when the global stress is close to the yield strength of the material. Lastly, another approach to categorise the residual stress relaxation mechanism has been outlined by Han et al. [16], where the relaxation behaviour has been classified into three regimes in relation to the magnitude of the stress ranges, $\Delta\sigma_n$, and the number of load cycles, N. According to this approach (much like the criteria proposed by James [10]), the relaxation of residual stresses principally occurs when the summation of the applied stress magnitude and the residual stress value exceeds the yield strength of the material. Subsequently, the other two loading regimes are the intermediate stress level, between

the yield and endurance limit, and finally the lower stress level below the fatigue endurance limit of the material. Furthermore, Han et al. [16] suggest that the residual stress redistribution is less pronounced in the intermediate and low stress regions compared to the high stress regime. Moreover, it is suggested that at intermediate stress levels, rapid residual stress relaxation will occur within the first few cycles while the relaxation behaviour at low stress levels below the endurance limit would depend on the material microstructure and dislocation pile ups. Therefore, the relaxation mechanism at low stress levels would be controlled by the micro-mechanical characteristics of the material whilst at high stresses the relaxation behaviour would depend on the macro-scale structural response of the material.

3 Residual stress redistribution under cyclic loading condition

3.1 A review of the past experimental and numerical studies

There are a number of studies conducted by other researchers in which the residual stress redistribution has been experimentally measured or numerically predicted [14], [15], [17]–[23]. The materials examined in the past studies together with the type of welding, specimen geometry, cyclic loading conditions such as stress amplitude and the load *R*-ratio, test frequency *f* and the number of fatigue cycles *N* are summarised in Table 1. Also included in this table are the key conclusions from each study. All the studies presented in Table 1 unanimously concluded that the residual stress relaxation is dependent on the fatigue loading conditions (i.e. stress amplitude and *R*-ratio) in the experimental studies and the hardening model in the numerical simulations. The results have shown that increasing the stress amplitude leads to a greater percentage of residual stress relaxation under cyclic loading conditions. Moreover, all of the past studies have shown that the largest percentage of residual stress relaxation occurs in the first fatigue cycle. In addition, using the simple hardening models, the relaxation is predicted to take place only in the first cycle whereas more complicated multilinear hardening models result in less considerable but continuous relaxation in further number of fatigue cycles at the beginning of the tests. Finally, it has been reported that the amount of residual stress relaxation is not equal in all directions and depending on the loading condition, the percentage of residual stress redistribution can be greater in one direction than the others.

Table 1: A summary of residual stress relaxation studies under cyclic loading conditions

Authors	Material	Type of welding	Loading Conditions	Type of Analysis	Total Number of Cycles	Key conclusions
V. Dattoma et al. [17]	AISI316	Longitudinal butt-weld joints with 3mm thickness	Stress amplitude: 53-106 MPa, *R*-ratio=0.1, f=10 Hz	Numerical analysis using bilinear isotropic hardening model	10 cycles	The residual stresses relaxation was limited to the first cycle.
D.J. Smith et al. [14]	En15R steel	Forged round bars	Axial tensile load	Residual stresses were measured using X-ray and hole drilling techniques and the relaxation was predicted using numerical analysis with simple linear and multilinear kinematic hardening models	Numerical analysis for 7 cycles	Using the linear kinematic hardening model, the residual stresses relaxed only in the first cycle. On the contrary, using the multilinear kinematic model, the relaxation occurred over multiple load cycles.
C. Cui et al. [18]	Q345 steel	Both-side welded rib-to-deck joints	Stress amplitude: 50-400 MPa, *R*-ratio=-2/3	Experimental study and numerical analysis using kinematic and nonlinear isotropic hardening models	10 cycles	The greatest part of residual stresses relaxation occurred in the first cycle and this relaxation stabilised after 5 loading cycles. With the increase of the applied stress amplitude, the extent of relaxation increased.
C.-H. Lee et al. [19]	SM400 steel	Two plates of 400×150×6 mm^3 welded with a single V-groove weld	Stress amplitude: 30-130 MPa, *R*-ratio=0.1	Numerical analysis using nonlinear kinematic hardening and isotropic hardening models	10 cycles	The distribution of residual stresses occurred only in the first few cycles. Residual stress relaxation was more pronounced in longitudinal direction compared to transverse direction.
J. Katsuyama et al. [20]	316L stainless steel	Pipe butt weld	Constant, increasing and decreasing stress amplitudes, negative and zero *R*-ratio, *f* =1 Hz	Numerical analysis using a bilinear kinematic hardening model	10 cycles	Residual stresses distributed during the first few cycles. The relaxation was more pronounced under a negative *R*-ratio compared to *R*=0.
J. Hensel et al. [15]	S355NL steel	Cruciform Joint	Stress amplitude: 100-140 MPa, *R*-ratio=-1 and 0	Numerical analysis	100 cycles	The greatest extent of residual stress relaxation occurred in the first ten cycles, with the maximum percentage observed in the first cycle. An increase in the stress amplitude resulted in a larger residual stress redistribution.
J. Cho et al. [21]	Duplex stainless steel - S32750	A single pass girth welding (single V-groove)	Stress amplitude: 100-300 MPa, *R*-ratio=-1	Numerical analysis with linear isotropic hardening and nonlinear kinematic hardening models	20 cycles	A greater relaxation was predicted at higher stress amplitudes.
X. Xie et al. [22]	316L stainless steel	Single overlay welding	Stress amplitude: 80 MPa, *R*-ratio=0.1, *f*=0.1 Hz	Experimental study and numerical analysis using nonlinear kinematic and isotropic hardening models	50 cycles	Roughly 45-60% of the initial maximum residual stresses were relaxed in the first load cycle. Further relaxation occurred in the next few cycles.
Z. Qian et al. [23]	AISI 1008, ASTM A572 and AISI 4142	600×100 mm^2 plates with different thickness	Various tensile stress amplitudes, *R*-ratio=0.1	Experimental analysis	10000 cycles for AISI 1008, 100 cycles for ASTM A572 and AISI 4142	Residual stress relaxation was observed only in transverse direction. A considerable relaxation occurred in the first fatigue cycle and no redistribution was observed in further cycles.

3.2 Residual stresses relaxation models

The researchers have attempted for many years to describe the relaxation of residual stresses under cyclic loading using different models. Each of the models presented in the literature is the result of empirical curve fitting of experimental data obtained from specific studies; therefore, some test specific constants must be determined for each case, which is analysed using these models. This means that there is no unique equation available in the literature to predict the redistribution of residual stresses for different types of joints and materials. In order to develop an understanding of the advantages and limitations of the existing models, each model has been briefly described, reviewed and discussed in this section with the view to identify the current gaps.

3.2.1. Morrow-Sinclair's model

Morrow-Sinclair (1959) [8] carried out an extensive study on cycle-dependent mean stress relaxation which is considered analogous to redistribution of residual stresses which occurs in structures subjected to fatigue loading conditions. They performed strain-controlled axial push-pull fatigue tests on SAE 4340 steel thin-walled tubes. They reported that the mean stress diminishes with increasing the number of cycles and this phenomena can be correlated with the material, the initial mean stress magnitude and the applied stress and strain amplitude [9]. In order to describe the mean stress relaxation under cyclic loading conditions without the need to measure them experimentally, due to the challenges involved in measurement of the locked-in stresses in structures, they proposed a model which was validated using the experimental data obtained from their study presented in Equation 1. As seen in this equation, the mean stress reduction due to residual stress redistribution is described as a function of the material's yield stress, stress amplitude, loading conditions and the number of fatigue cycles. Moreover, experimental data are required to identify the material dependent constant in this model. It is important to highlight that Equation 1 has been derived for the test data which were obtained at the load ratio of R= -1 (i.e. fully reversed cycles), therefore the proposed model by Morrow-Sinclair cannot be used for other values of R-ratio [24].

$$\frac{\sigma_{mN}}{\sigma_{m1}} = \frac{\sigma_y - \sigma_a}{\sigma_{m1}} - \left(\frac{\sigma_a}{\sigma_y}\right)^b \times \log(N) \qquad \text{Equation 1}$$

where σ_{mN} is the mean stress measured after N cycles, σ_{m1} is the mean stress measured at the first cycle, σ_y is the yield stress of the material, σ_a is the stress amplitude, b is a constant which depends on the material softening behaviour and the applied strain range $\Delta\varepsilon$, and N is the number of fatigue cycles.

3.2.2. Impellizzeri's model

Impellizzeri (1970) [25] developed a model using a first-order approximation in order to carry out a study on fatigue damage analysis in the presence of residual stresses. Hence, a simple exponential function was proposed to predict the redistribution of residual stresses even below the endurance limit at the notch root which is presented in Equation 2. As seen in this equation, the residual stress relaxation depends on the material's yield stress, loading conditions and number of cycles. Moreover, some experimental data are needed to identify the material dependent constant in this model.

$$r_N = r_0 \times e^{\frac{-a \times N \times \varepsilon_R \times \sigma_R}{\sigma_y}} \qquad \text{Equation 2}$$

where r is the value of residual stress after N cycles, r_0 is the initial residual stress value, a is a material index which has to be determined empirically, N is the number of fatigue cycles, ε_R is the applied strain range at the notch root, σ_R is the applied stress range at the notch root and σ_y is the yield stress of the material.

3.2.3. Jhansale-Topper's model

Jhansale-Topper (1973) [26] performed a study to predict the mean stress relaxation under cyclic loading conditions, similar to that previously conducted by Morrow-Sinclair [9]. The Jhansale-Topper's model is presented in Equation 3. As seen in this equation, the model proposed by Jhansale-Topper is simply dependent on the initial state of the mean stress, the number of fatigue cycles and a constant, which depends on the material and loading conditions. Jhansale-Topper's model suggests that the mean stress relaxes at an exponential rate in relation to the number of fatigue cycles and that the higher strain ranges result in a greater mean stress relaxation. Moreover, the relaxation rate has not been limited to the direction of mean stress, hence this model has been proposed for both tensile and compressive mean stresses.

$$\sigma_{o_N} = \sigma_{o_1} \times N^r \qquad \text{Equation 3}$$

where σ_{o_1} is the absolute value of initial mean stress, σ_{o_N} is the absolute value of mean stresses after N cycles, N is the number of fatigue cycles and r is the relaxation exponent which is considered to be a function of the applied strain range.

Landgraf and Chernenkoff (1988) [27] proposed an improved version of the Jhansale-Topper's model by determining the value of the exponent in relation to a threshold strain range $\Delta\varepsilon_{th}$ below which the redistribution of residual stresses is considered to be negligible. According to their model, the residual stress relaxation is described as a function of material properties (i.e. hardness) and the strain threshold value, which depends on the examined material.

$$r = 8.5 \times 10^{-2}\left(1 - \frac{\Delta\varepsilon}{\Delta\varepsilon_{th}}\right) \qquad \text{Equation 4}$$

$$\frac{\Delta\varepsilon_{th}}{2} = e^{(-8.41+5.36\times10^{-3}\times HB)} \qquad \text{Equation 5}$$

where $\Delta\varepsilon$ is the applied strain range, $\Delta\varepsilon_{th}$ is the threshold strain range and HB is the Brinell hardness value.

3.2.4. Potter's model

Potter **(**1973) [28] performed a comprehensive study on the effect of load interactions under fatigue loading conditions in order to calculate the contribution of cycle-dependent local stresses to fatigue damage accumulation. Potter's model is presented in Equation 6. According to Potter's model, the non-equilibrium component of the residual stress must be taken into consideration for the cycle-dependent relaxation analysis. Conversely, this model suggests that the other part of residual stress, which is the equilibrium component, is generated only in the presence of nominal loads [28]. It is important to highlight that the residual stress variation due to cyclic loading condition in Potter's model has been considered as a phenomenon which is analogous to a transient behaviour found in critically damped systems [28].

$$\sigma_{transient} = A \times e^{B \times N} \quad \text{Equation 6}$$

where $\sigma_{transient}$ is the non-equilibrium component of the residual stress, A, B are constants to be determined by applying appropriate boundary conditions and N is the number of fatigue cycles.

3.2.5. Iida's model

Iida (2000) [29] investigated the relaxation behaviour of residual stresses in butt-welded specimens and proposed a model to described the residual stress redistributions in longitudinal direction which is presented in Equation 7. As seen in this equation, according to Iida's model the longitudinal residual stresses in welded joints redistribute as a function of the number of loading cycles and the material dependent constants that need to be quantified experimentally.

$$\sigma_{RY} = A + B \times \mathrm{Log}(N) \qquad 1 \leq N \leq 10^4 \quad \text{Equation 7}$$

where σ_{RY} is the longitudinal residual stress, N is the number of fatigue cycles and A, B are empirical constants which need to be determined experimentally.

3.2.6. Han's model

Han (2002) [16] performed a study on residual stress redistribution under fatigue loading conditions and proposed a model which is presented in Equation 8 and Equation 9. According to Han's model, the residual stress relaxation behaviour primarily depends on the summation of initial residual stress value and the applied stress level. Based on his model, two distinct equations are proposed to predict the residual stress relaxation depending on whether the summation of initial residual and applied stresses is below or above yield stress of the material. According to this model, the distinction between the total stress values or below and above yield is due to the fact that when the summation of residual and applied stresses is lower than the yield stress, the relaxation occurs because of micro-plastic deformations that are induced due to stress concentration and strain hardening [16].

$$\frac{\sigma_{res_{ini}} + \sigma_{app}}{\sigma_y} < 1, \qquad \sigma_{res_{relax}} = \sigma_{res_{ini}} \times N^{-k} \quad \text{Equation 8}$$

$$\frac{\sigma_{res_{ini}} + \sigma_{app}}{\sigma_y} > 1, \quad \sigma_{res_{relax}} = \sigma_{res_{ini}} \left[-1.6 \left(\frac{\sigma_{res_{ini}} + \sigma_{app}}{\sigma_y} \right) + 2.6 \right] N^{-k} \quad \text{Equation 9}$$

where $\sigma_{res_{ini}}$ is the initial residual stress value, $\sigma_{res_{relax}}$ is the residual stress value after N cycles, σ_{app} is the applied stress, σ_y is the yield stress of the material, N is the number of fatigue cycles and k is a material dependent constant that needs to be determined from the experimental data.

3.2.7. Xie and Qian's model

Xie *et. al.* [21] and Qian *et. al.* [22], [23] performed similar studies to predict the value of residual stress for each load cycle under fatigue loading conditions using the equation shown in Equation 10 and Equation 11. It is important to highlight that this equation has been developed based on the hypothesis that the residual stress relaxation can be considered analogous to the time-dependent creep deformation of engineering materials, as suggested by Valluri [30]. According to this hypothesis, residual stresses and creep deformation both introduce a variation in stress or strain over time in the presence of external loads [23]. Therefore, these two time-dependent mechanisms have been assumed to be in a comparable analogy.

$$S = \left[a\left(\frac{\sigma_a}{\sigma_y}\right)^n + b\right] \times [\log(N+1)]^m \quad \text{Equation 10}$$

$$\sigma_N = \sigma_0(1 - S) \quad \text{Equation 11}$$

where S is the attenuation ratio, σ_a is the applied stress amplitude, σ_y is the yield stress of the material, σ_N is the residual stresses value after N cycles, σ_0 is the initial residual stress value, N is number of load cycles and a, b, n, m are material constants which are obtained from the equation of the line of best fit to the experimental data. Moreover, in Equation 11, σ_N is the residual stress value for a given number of fatigue cycle and σ_0 is the initial residual stress value.

The disadvantages and weaknesses of Xie and Qian's model have been explained and discussed by Wang et al. [31]. In particular, it has been noted in the study by Wang et al. [31] that Equation 11 should not be used for ferritic steels and aluminium alloys due to negligible creep deformation at low temperatures. Moreover, the common concept that the redistribution of residual stresses mainly occurs when the total stress exceeds the yield stress of the material is considered to be inaccurate because the yield strength may vary in different locations of the welded joint due to the microstructural heterogeneity [31]. Finally, it is noteworthy to mention that Xie and Qian's model doesn't consider the cold working effects on the residual stress distributions. Therefore, more complicated models such as those proposed by Zhuang et al. [24] and Zaroog et al. [32] need to be developed to account for the machining and fabrication effects on the residual stress behaviour of the welded structures.

As shown above, there are a number of empirical models available in the literature to predict the residual stresses redistributions under cyclic loading conditions and therefore calculating the fatigue life of an engineering structure with higher accuracy. However, due to the complexity involved with the welding process, it is difficult to define a general equation to be used for all types of materials and welded joints. As seen in this section, the proposed models by other researchers are dependent on a number of key parameters, which include the number of fatigue cycles, the type of weld, initial residual stress value, applied stress amplitude, the yield strength of the material and material dependent constants obtained from the experimental data. Therefore, there is need to perform finite element simulations to predict the residual stress relaxation behaviour in OWT monopiles by considering the appropriate material and loading conditions in numerical studies.

4 Finite element modelling of residual stresses redistribution

In order to predict the residual stress redistribution in offshore wind welded structures, such as monopile foundations, weld simulations have been performed and the sensitivity of the residual stress relaxation to the applied stress amplitude level has been examined. The material examined in this study is S355 structural steel, which is widely used in fabrication of offshore structures, including OWT monopiles. To provide an overview of the most common methodology to introduce residual stress profiles in weld simulations, the thermo-mechanical procedure is described first, followed by the model set up. Residual stress prediction results are presented at the end.

It is worth noting that the welded plate modelled in the present study uses a thinner section (as compared to the plate thicknesses used in OWT monopile weldments) for developing the finite element model. Such a simplification would significantly reduce the number of elements, hence lead to lesser computational power and time requirements. Albeit, the simulation results would reveal the

interaction of fatigue loading conditions on residual stress profile in the weld cross-section. Further research will be conducted in future work to run weld simulations on thicker components with the exact dimensions of the OWT monopiles.

4.1 Thermo-mechanical analysis

For the purpose of applying the residual stresses in the finite element weld simulation, it is necessary to define the equations which describe the thermal analysis related to the welding process and the subsequent thermal stress analysis as a result of temperature distributions [33]. In particular, the thermal analysis is necessary to work out the transient temperature history, which is the result of heat flow of the welding process induced by the torch. In the next step, the stress analysis uses the temperature fields as the source of thermal loading and introduce welding residual stresses in the model [33]. Hence, the estimation of the residual stresses pattern is highly dependent on the accuracy of the heat source geometry and the model used for describing the behaviour of the material [34].

4.1.1 Thermal Analysis

The first mathematical model describing the evolution of the heat source during the welding process was proposed by Rosenthal [35] in 1946. A more advanced model was developed by Goldak et al. [36] in 1984, which has been the basis of many of the weld simulation studies. This model implements a double ellipsoidal geometry distribution of the heat source in order to allow the user to easily modify the size and the shape of it. This is an essential feature since in a welding process the depth of the arc penetration can vary in relation to the thickness of the components. Moreover, using Goldak's approach it is possible to perform accurate analyses even on non-axisymmetric and spherical symmetry geometries [36].

According to Goldak's proposed model, two separate heat sources are defined for the front half and the rear part of the double ellipsoidal power density distribution, which are described below [36]:

Front: $$q(x,y,z,t) = \frac{6\sqrt{3}f_f Q}{a_1 bc\pi\sqrt{\pi}} e^{-3(z-vt-z_0)^2/a_1^2} e^{-3x^2/b^2} e^{-3y^2/c^2}$$ Equation 12

Rear: $$q(x,y,z,t) = \frac{6\ \sqrt{3}f_r Q}{a_2 bc\pi\ \sqrt{\pi}} e^{-3(z-vt-z_0)^2/a_2^2} e^{-3x^2/b^2} e^{-3y^2/c^2}$$ Equation 13

where f_r and f_f are constants which define the portion of the heat deposited in the rear and front parts, respectively, Q is the magnitude of the input heat per unit time, v is the speed of the welding process, t is the time of the welding process, z_0 is the initial position of the heat source in the z-axis, and a_1, a_2, b, c are constants which have to be defined in relation to the features of the welding arc.

4.1.2 Stress Analysis

A detailed analysis of the stress distribution in weld simulation by Lindgren [37]–[39] has shown that the main challenge in weld simulations is not imposed by the complex material behaviour but it is often the lack of accurate material properties at high temperatures. A review of the previous studies on this topic, including the research conducted by Xie et al. [22], Cho et al. [21] and Lee et al. [33], shows that the three main models which need to be implemented in stress analysis of weld geometries are the initial yield criterion, plastic flow rule and material hardening model.

The initial yield criterion is necessary to delineate the conditions for the onset of plastic strain [21] and can be described by [21], [22]:

$$F = f(\sigma - \alpha) - \sigma^0 = 0 \qquad \text{Equation 14}$$

where $f(\sigma - \alpha)$ is the equivalent von Mises stress with respect to the back stress α and σ^0 is the radius of the initial yield surface.

The plastic flow rule is needed to define the direction of the plastic deformation flow increment after the yield limit of the material has reached. Finally, the hardening model is used to determine the changes in the yield surface as a result of plastic deformation. It is important to mention that there is a material model developed by Chaboche et al. [40], [41], which is commonly used in numerical simulations of the welding process [15], [18], [33], [42]. This model is composed of an isotropic hardening part and a nonlinear kinematic hardening part and enables the implementation of many physical phenomena such as ratcheting, redistribution of mean stresses and cyclic hardening characteristic in the presence of cyclic loads [42]. In this model, the isotropic component is needed to describe the expansion of the yield surface while the kinematic component describes the translation of the yield surface in deviatoric stress space with increasing plastic strain [33]. In the present study, an isotropic hardening model has been implemented by employing the stress-strain curve of S355 material [4], which gives the half cycle hardening behaviour.

4.2 Finite element model set-up

A sequentially coupled thermal stress analysis followed by an additional cyclic loading step was conducted on a single V-grove plate (autogenous weld) in the commercial finite element software ABAQUS®, to study the redistribution behaviour of the weld residual stresses under cyclic loads. The details of the model has been described below.

4.2.1 Geometry, material and mesh design

A 3-dimensional (3D) plate geometry of 100 mm length, 30 mm width and 12 mm thickness was built in ABAQUS®. The part geometry was partitioned before assigning temperature dependent material properties from Table 2. The dimensions of the designed plate and the partitioning strategy are demonstrated in Figure 2: Single V-groove weld plate geometry (a) front view, (b) 3D view . As seen in this figure, a partition was assigned to the centre of the weld region in order to extract and report the residual stress distribution with respect to the centreline of the weld.

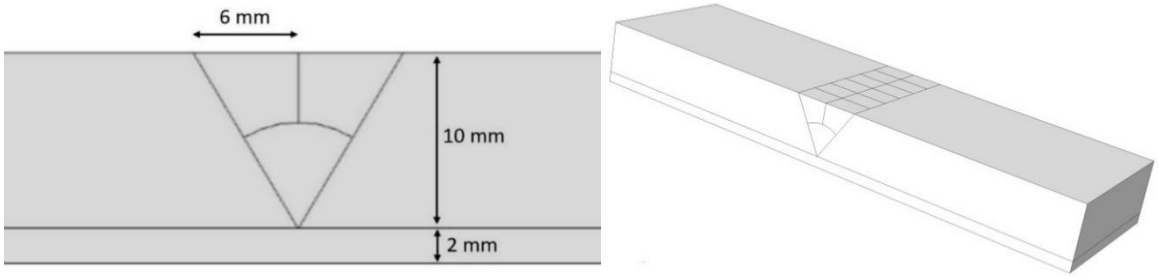

Figure 2: Single V-groove weld plate geometry (a) front view, (b) 3D view

Although weld metal and base metal are known to exhibit different material properties, in the present model, the same properties were assigned to the base and weld metal. The material used in this study is S355 steel, which is widely used in fabrication of offshore structures including OWT foundations [43]–[45]; Temperature-dependent material properties for S355 steel reported by Outinen et al. [46] were employed in the model as summarised in Table 2: S355 material properties at different

temperatures [46]. The use of temperature-dependent material property helps to capture the differential response of the weld metal and base metal.

Table 2: S355 material properties at different temperatures [46]

Temperature [°C]	**Thermal conductivity [W/m×K]**	**Density [kg/m^3]**	**Young's modulus [GPa]**	**Poisson's ratio**	**Thermal expansion coefficient [1/K]**	**Yield stress [MPa]**	**Heat input [J/g×K]**
20	55	7.15	210	0.27	1.17×10^{-5}	539	0.501
200	50	7.05	189	0.27	1.17×10^{-5}	522	0.590
300	46	7.00	168	0.27	1.17×10^{-5}	512	0.619
400	42	6.95	147	0.27	1.17×10^{-5}	458	0.669
500	39	6.90	126	0.27	1.17×10^{-5}	350	0.719
600	34	6.85	65	0.27	1.17×10^{-5}	172	0.784

Due to the complexity of the sequentially coupled thermal stress simulations, a relatively coarse but structured mesh was assigned to the geometry as shown in Figure 3: The finite element mesh applied to the part geometry. 8-noded linear hexahedral elements, DC3D8 and C3D8, were assigned to the geometry for the thermal and stress analysis models respectively. The finite element size was 2×2×2 mm^3. In total, there were 5340 elements in the weld geometry. As shown in Figure 3: The finite element mesh applied to the part geometry, an attempt was made to design a mesh geometry with an aspect ratio close to unity to avoid numerical errors in the weld simulations. It is worth noting that, although it has not been shown here for brevity, a mesh sensitivity analysis was conducted and 2×2×2 mm^3 was found to be the optimum element size for the present study.

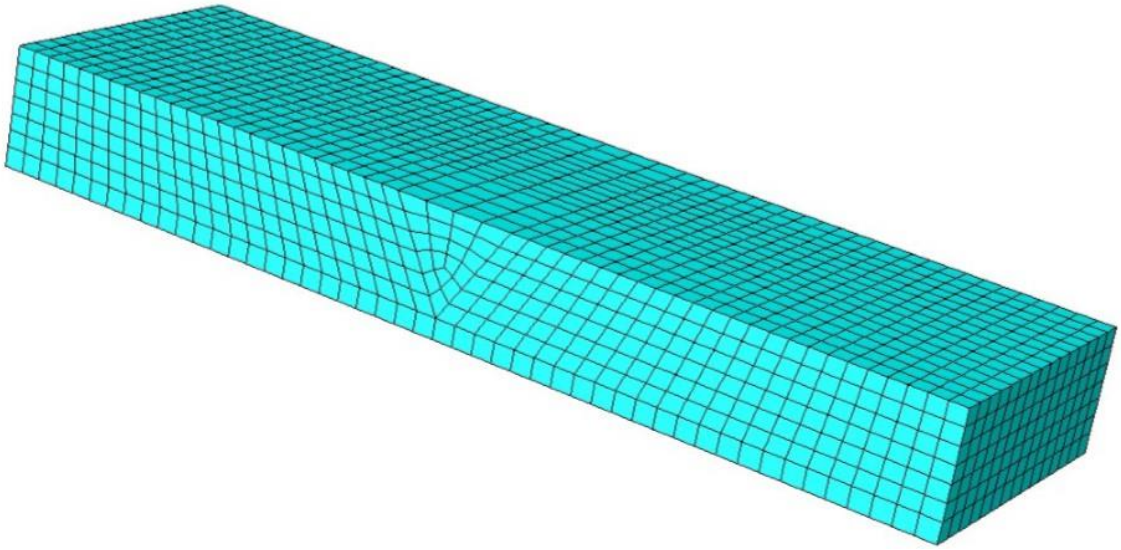

Figure 3: The finite element mesh applied to the part geometry

4.2.2 Welding parameters

After the creation of the geometry, the weld simulation was conducted using the "ABAQUS Welding Interface" plug-in. The heat flux and peak temperatures were assigned to the cells representing the deposited weld metal (i.e. region within the V-groove, refer Figure 2) in the model. In order to simulate individual weld beads, the "chunking method" was adopted for defining the so-called "chunks". This helps in modelling the progressive addition of the elements representing the deposited beads. Furthermore, the "cell extrusion" technique was used as a chunking method by considering

one cell per chunk. Hence, for the geometry examined in this study, 3 weld beads were created with 6 chunks in each bead.

After the creation of the beads and chunks, the definition of the so-called "weld passes" was required to describe the behaviour of the chunks during the simulation. Therefore, for each chunk created in the model, an ABAQUS step is automatically generated by the plug-in with the help of DFLUX subroutine. Furthermore, the torch boundary temperature function was linearly ramped up to reach the target torch temperature and begin the material deposition. When the weld metal is deposited in each pass, the plug-in activates the FILM and GAPCON subroutines to update the boundary condition. The boundary condition, in this case, is represented by the interface between the base material and the weld bead. The film coefficient was set to $0.025\ [W/mm^2 \times K]$ and the sink temperature was fixed at $21.1\ [°C]$ while other parameters were set to the default values. In this analysis, 18 weld passes (3 beads and 6 chunks) were simulated in total.

The weld simulation was carried out following the approach explained above and a sequence of weld beads were deposited in the V-groove of the S355 plate as shown in Figure 4. As seen in this figure, the heat transfer analysis was performed to predict the temperature distribution across the plate during the welding process. This gives the inputs for the predefined temperature fields and residual stresses for the welded plate, which can be further subjected to cyclic loading to study the residual stress relaxation behaviour as a function of the applied fatigue cycles.

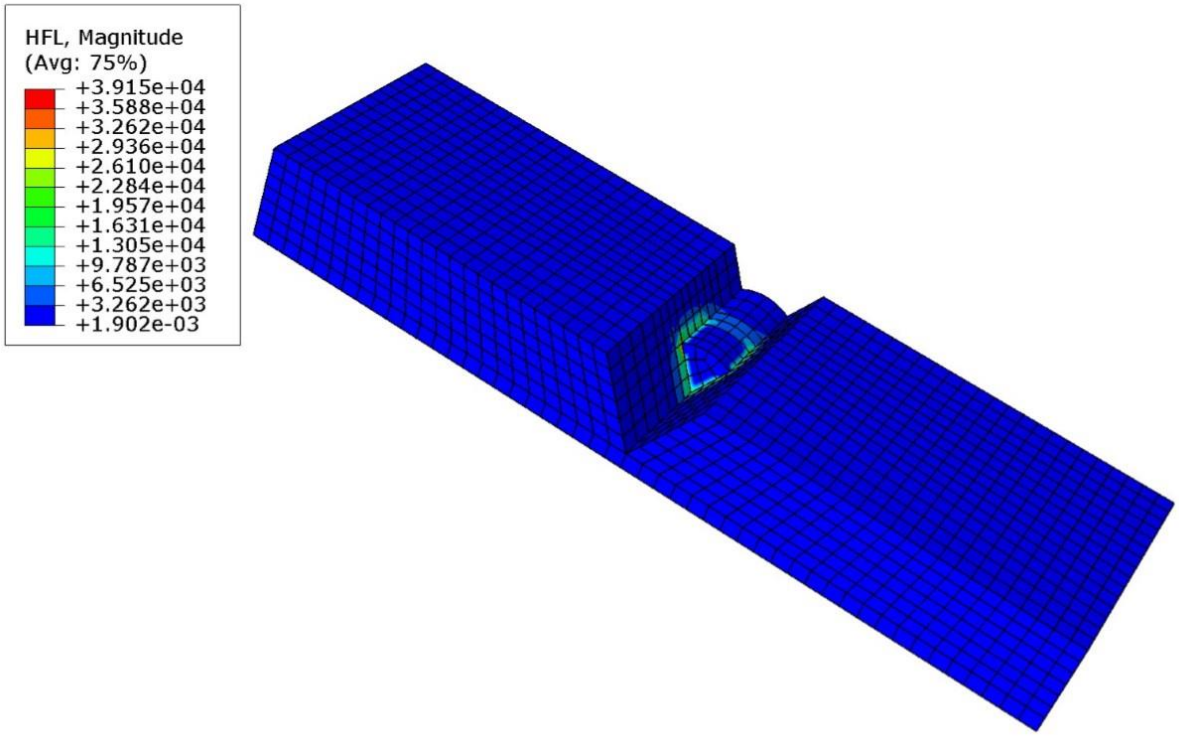

Figure 4: Heat transfer analysis in the weld simulation

4.2.3 Applied load and boundary conditions

The numerical steps explained so far were to conduct the weld simulations (sequential thermal stress analysis) and predict the initial state of residual stresses in the welded plate. However, in order to predict the residual stress redistribution under cyclic loading, further boundary conditions were applied in the model to replicate the fatigue loading conditions. Therefore, a pressure load was applied

to one end of the geometry in addition to the following boundary conditions as shown in Figure 5: Illustration of the boundary conditions and pressure load applied to replicate tensile cyclic stresses in the weld geometry :

1) ZSYMM (U3=UR1=UR2=0) on the front surface and the back surface
2) U1=0 on one end of the weld geometry, opposite to the end where the load is applied.
3) U2=0 at the bottom left corner of the side surface opposite to the end where the load is applied

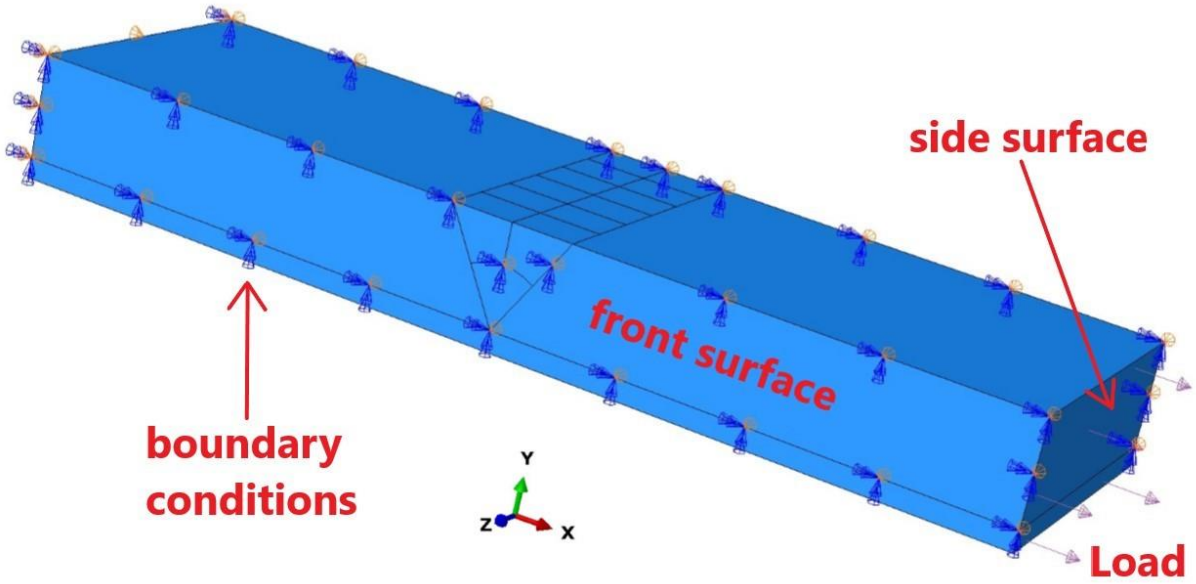

Figure 5: Illustration of the boundary conditions and pressure load applied to replicate tensile cyclic stresses in the weld geometry

Figure 6Since an OWT is subjected to wave and wind loads of varying amplitudes throughout its lifetime, the loads can be grouped into a finite number of sinusoidal load cases of individual frequencies (using rainflow counting method) and used in the fatigue analysis of OWT structures [47]. Therefore, a sinusoidal waveform with a time period of 300 s was applied in the model as presented in Figure 6. As seen in this figure, a fully reversed cycle with *R*-ratio of -1 was defined. Finally, in order to predict the residual stress redistribution under different stress amplitudes, five different load cases were examined in finite element simulations with the maximum stresses ranging from 15 MPa to 60 MPa.

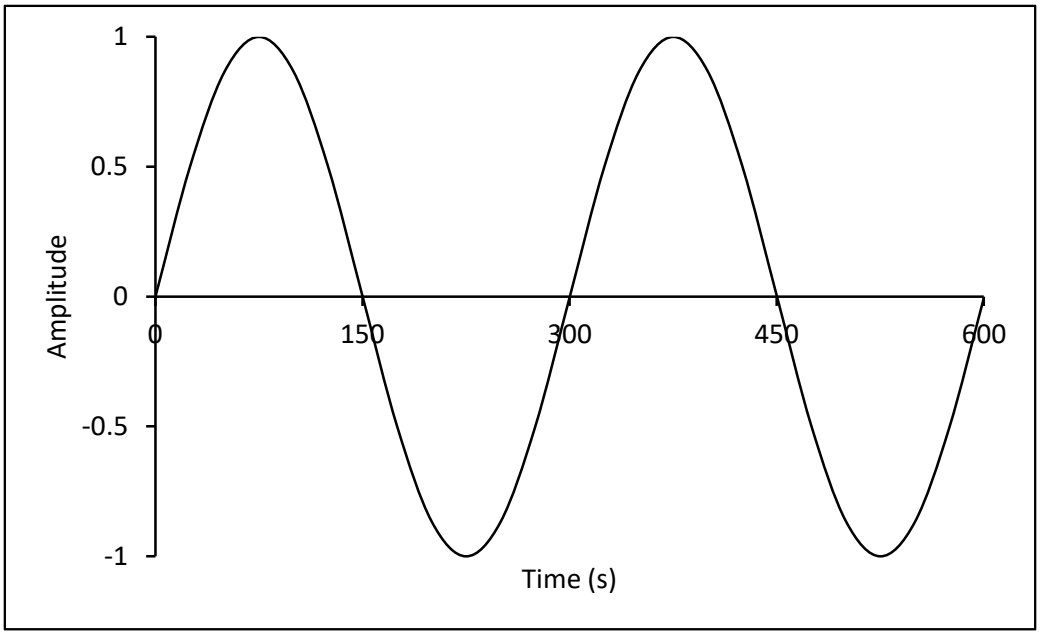

Figure 6: Sinusoidal fatigue waveform

4.3 Residual stress redistribution results and discussion

Upon completion of the weld simulation, the initial residual stress distribution profile in transverse direction was extracted from the centreline of the weld region. It is worth noting that, in OWT monopiles, the operational loading condition is such that the principal stress direction acting on the circumferential welds, which provides the driving force for fatigue crack initiation and propagation, is along the axial direction of the monopile geometry. Therefore, transverse residual stresses were extracted from the weld simulation models and analysed in the present study. As shown in Figure 7, the data extraction process was conducted by defining a path starting in the middle of the weld and ending 40 mm away from the centreline of the weld.

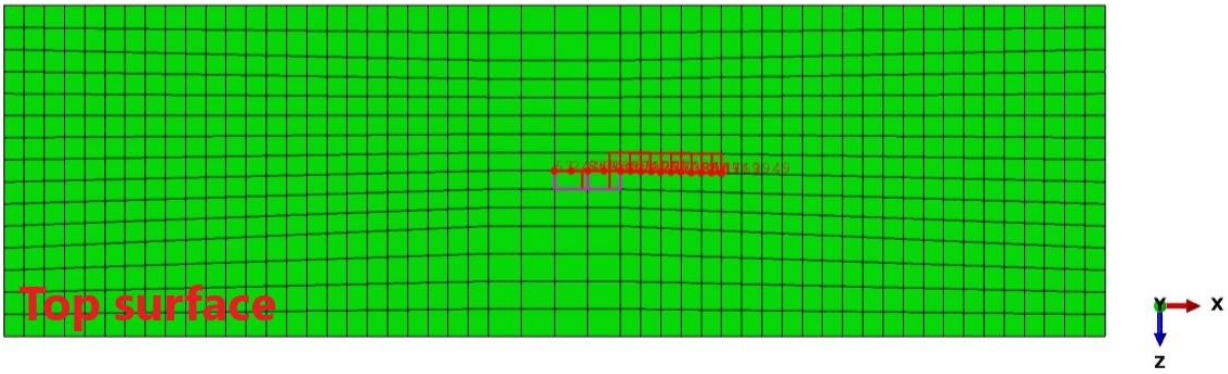

Figure 7: The defined path for extracting the residual stress distribution profile from the weld simulation model

The transverse residual stress prediction results from the initial weld simulation and the subsequent simulations in the presence of a range of applied stresses (15 MPa-60 MPa) are presented and compared with each other in Figure 8: Residual stress relaxation results. It can be clearly seen that the level of residual stress relaxation is directly proportional to the applied stress level, within the first

fatigue cycle, and the greatest percentage of residual stress relaxation has occurred for the load case with the highest stress level. The residual stress relaxation trends clearly demonstrate that under a single fatigue loading cycle, a relatively large stress level can significantly relax the peak residual stresses by bringing them down close to zero. It is also interesting to note that the residual stress relaxation under cyclic loading condition has appeared to occur both in the tensile and compressive components of residual stress. The results in Figure 8: Residual stress relaxation results show that, within a reasonably large distance from the centreline of the weld region (i.e. 40 mm in the examined weld geometry), the tensile residual stresses (which have a damaging effect on the structural integrity of OWT monopiles) tend to continuously decrease in magnitude. Further analysis of the residual stress redistribution results has been presented in Figure 9, where the relaxation of the peak tensile stress at the centre of the weld region was plotted against the applied stress level. As seen in this figure, the peak tensile residual stress decreases with increasing levels of applied stress amplitude. Cyclic load with 60 MPa maximum stress value showed 88% reduction in the residual stress while the plate subjected to cyclic load with 15 MPa maximum stress value exhibited a 33% reduction in the residual stress.

The results in Figure 10 show the response of the welded plate with respect to applied number of cycles, under a 50 MPa stress amplitude. It can be observed that, under the examined stress level, the greatest reduction in transverse residual stress at the centreline of the weld was observed in the first cycle while a negligible amount of further relaxation was seen within the following two cycles. Also seen in this figure is that increasing the number of fatigue cycles beyond three, does not seem to have any effect on the residual stress redistribution profile at the centreline of the weld. These prediction results are consistent with the findings from other studies summarised in Table 1. It is known that depending on the soil condition and subsequently the required hammering loads, a severe fatigue life depletion is accounted for upon completion of the OWT monopiles installation phase. However, the obtained results in Figure 8: Residual stress relaxation results and Figure 9 imply that, although the hammering loads during the pile driving phase have a detrimental effect on the fatigue life, they can also improve the residual life of the OWT monopiles due to the shake down hence relaxation of damaging tensile residual stresses in transverse direction with respect to the weld geometry. The presented finite element results in this study are based on isotropic hardening model, therefore more complex hardening models will be employed in future work to improve the accuracy of the prediction results similar to other studies reported in Table 1. Another area of research to be investigated in future work is the weld simulation of thicker plates with double V-grooves to replicate the realistic dimensions of the OWT monopiles. It is known that the monopiles can have large thicknesses in the excess of 100 mm [6]. Therefore, the influence of plate thickness and size effect on the residual stress relaxation behaviour of monopile weldments will be examined and compared with experimental measurements in future work.

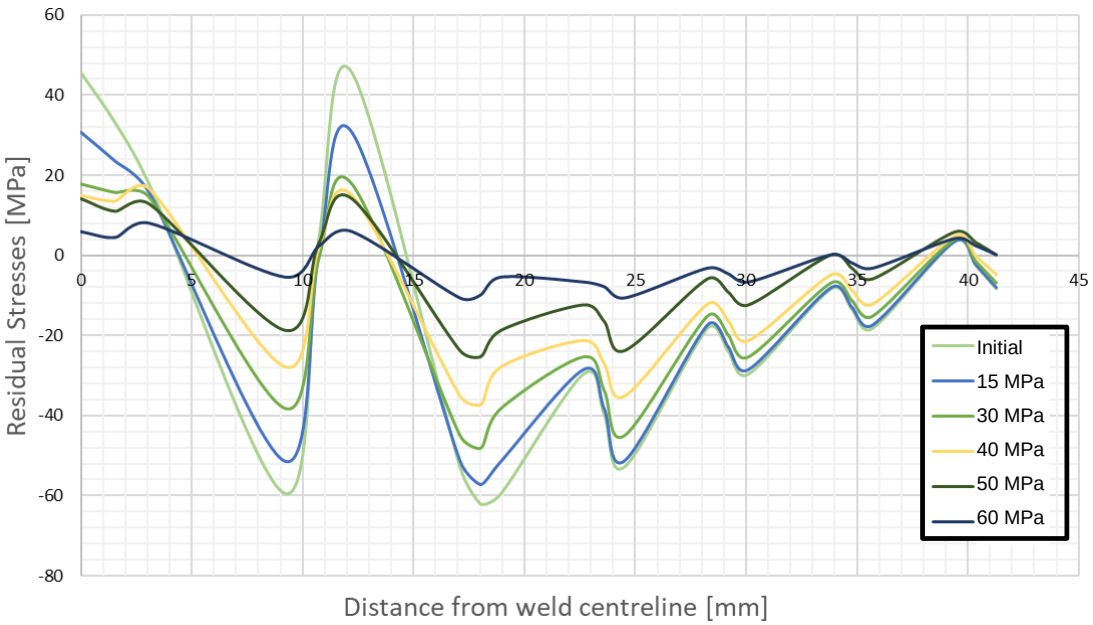

Figure 8: Residual stress relaxation results after applying the first fatigue cycle with different stress levels

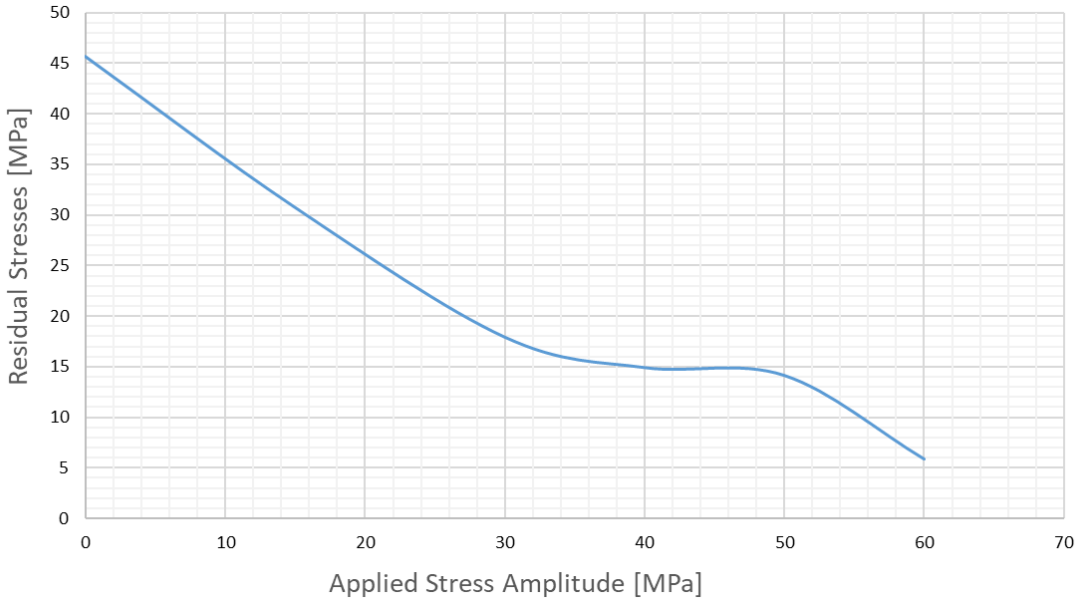

Figure 9: Relaxation of initial tensile residual stress against the applied stress level

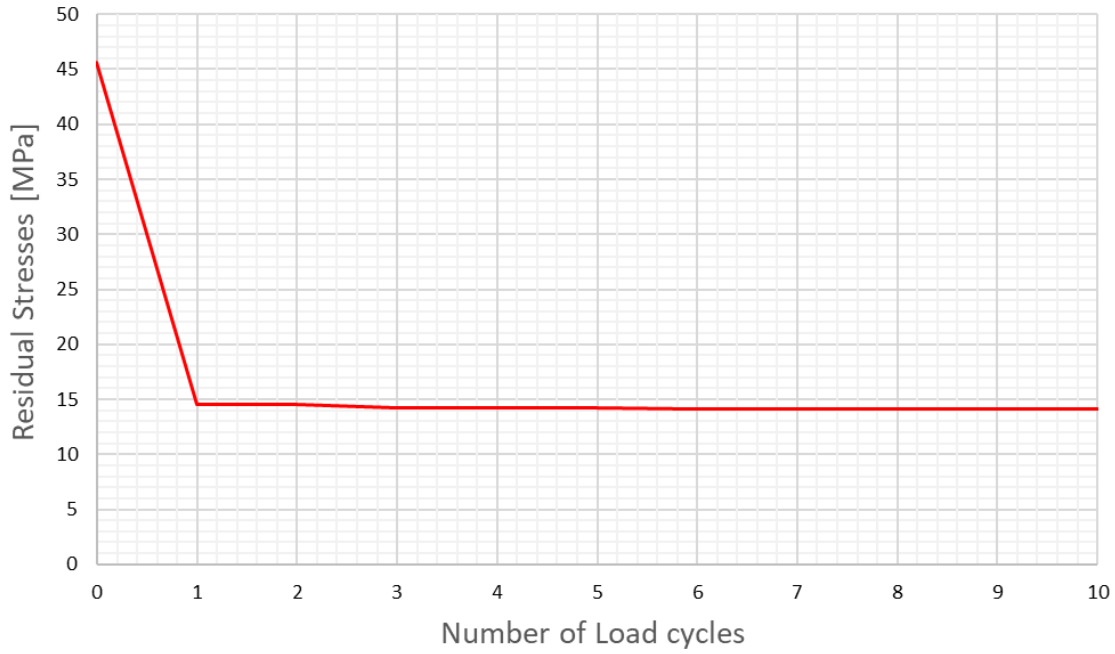

Figure 10: The effect of number of fatigue cycles on residual stress relaxation at the centre of the weld under 50 MPa

5 Conclusions

The aim of this study was to evaluate the effect of cyclic loading on residual stress redistribution behaviour in offshore wind welded structures, including OWT monopile foundations. The existing empirical models available in the literature showed that residual stresses redistribute under cyclic loading conditions, particularly in the first few cycles. Although all the existing models show a strong dependency on material properties and loading conditions, such as stress amplitude and *R*-ratio, none of the current models provided a general equation describing the residual stress relaxation for a wide range of materials and loading conditions. Therefore, finite element simulations were conducted in this study to predict the sensitivity of residual stresses in OWT monopiles to the cyclic loading conditions. Weld simulations have been conducted using a sequentially coupled thermal stress analysis approach available in ABAQUS Welding Interface. The initial state of residual stress profiles in a simplified single V-groove welded structure was modelled. Subsequently, fatigue loading conditions with *R* ratio of -1 and a range of stress levels have been applied to the modelled structure to predict the residual stress relaxation behaviour. The finite element results have shown that the largest percentage of residual stress relaxation occurs in the first fatigue cycle with the following cycles having negligible effects on residual stress redistribution. The results have also shown that, if the applied stress level is sufficiently large, the residual stresses can be almost entirely released from the welded structure after the first fatigue cycle. The predicted results imply that, while the hammering loads during the pile driving process induce fatigue damage into monopiles, they have a significant beneficial effect on the structural integrity of monopiles by shaking down the damaging residual stresses. Further research will be conducted in future to perform simulations on more complex double V-grooved welded geometries with larger thicknesses, similar to true dimensions of monopile structures, to investigate the residual stress redistributions due to fatigue cycles.

REFERENCES

[1] "Oil, gas and coal - Ensuring the efficient and responsible use of fossil fuel," European Commission. [Online]. Available: https://ec.europa.eu/energy/en/topics/oil-gas-and-coal. [Accessed: 28-Jul-2019].

[2] E. Sesto and N. H. Lipman, "Wind energy in Europe," Wind Eng., vol. 16, no. 1, pp. 35–47, 1992.

[3] Wind Europe, "Offshore wind in Europe," Refocus, pp. 1–37, 2018.

[4] A. Jacob, J. Oliveira, A. Mehmanparast, F. Hosseinzadeh, J. Kelleher, and F. Berto, "Residual stress measurements in offshore wind monopile weldments using neutron diffraction technique and contour method," Theor. Appl. Fract. Mech., 2018.

[5] J. Velarde, "Design of Monopile Foundations to Support the DTU 10 MW Offshore Wind Turbine," no. June, 2016.

[6] M. Bocher, A. Mehmanparast, J. Braithwaite, and M. Shafiee, "New shape function solutions for fracture mechanics analysis of offshore wind turbine monopile foundations," Ocean Eng., 2018.

[7] C. Sun and V. Jahangiri, "Fatigue damage mitigation of offshore wind turbines under real wind and wave conditions," Eng. Struct., 2019.

[8] A. Jacob, A. Mehmanparast, R. D'Urzo, and J. Kelleher, "Experimental and numerical investigation of residual stress effects on fatigue crack growth behaviour of S355 steel weldments," Int. J. Fatigue, 2019.

[9] J. Morrow and G. Sinclair, "Cycle-Dependent Stress Relaxation," in Symposium on Basic Mechanisms of Fatigue, ASTM International, 2009, pp. 83-83–27.

[10] M. R. James, RELAXATION OF RESIDUAL STRESSES - AN OVERVIEW. 1987.

[11] V. Igwemezie and A. Mehmanparast, "Waveform and frequency effects on corrosion-fatigue crack growth behaviour in modern marine steels," Int. J. Fatigue, 2020.

[12] V. Igwemezie, A. Mehmanparast, and A. Kolios, "Current trend in offshore wind energy sector and material requirements for fatigue resistance improvement in large wind turbine support structures – A review," Renewable and Sustainable Energy Reviews. 2019.

[13] V. Igwemezie, A. Mehmanparast, and A. Kolios, "Materials selection for XL wind turbine support structures: A corrosion-fatigue perspective," Mar. Struct., 2018.

[14] D. J. Smith, G. H. Farrahi, W. X. Zhu, and C. A. McMahon, "Experimental measurement and finite element simulation of the interaction between residual stresses and mechanical loading," Int. J. Fatigue, 2001.

[15] J. Hensel, T. Nitschke-Pagel, D. Tchoffo Ngoula, H. T. Beier, D. Tchuindjang, and U. Zerbst, "Welding residual stresses as needed for the prediction of fatigue crack propagation and fatigue strength," Eng. Fract. Mech., 2018.

[16] S. Han, T. Lee, and B. Shin, "Residual stress relaxation of welded steel components under

cyclic load," Steel Res., 2002.

[17] V. Dattoma, M. De Giorgi, and R. Nobile, "Numerical evaluation of residual stress relaxation by cyclic load," J. Strain Anal. Eng. Des., 2004.

[18] C. Cui, Q. Zhang, Y. Bao, S. Han, and Y. Bu, "Residual stress relaxation at innovative both-side welded rib-to-deck joints under cyclic loading," J. Constr. Steel Res., 2019.

[19] C. H. Lee, V. N. Van Do, and K. H. Chang, "Analysis of uniaxial ratcheting behavior and cyclic mean stress relaxation of a duplex stainless steel," Int. J. Plast., 2014.

[20] J. Katsuyama, Y. Yamaguchi, Y. Li, and K. Onizawa, "Effect of cyclic loading on the relaxation of residual stress in the butt-weld joints of nuclear reactor piping," Nucl. Eng. Des., 2014.

[21] J. Cho and C. H. Lee, "FE analysis of residual stress relaxation in a girth-welded duplex stainless steel pipe under cyclic loading," Int. J. Fatigue, 2016.

[22] X. fang Xie, W. Jiang, Y. Luo, S. Xu, J. M. Gong, and S. T. Tu, "A model to predict the relaxation of weld residual stress by cyclic load: Experimental and finite element modeling," Int. J. Fatigue, 2017.

[23] Z. Qian, S. Chumbley, T. Karakulak, and E. Johnson, "The residual stress relaxation behavior of weldments during cyclic loading," Metall. Mater. Trans. A Phys. Metall. Mater. Sci., 2013.

[24] W. Z. Zhuang and G. R. Halford, "Investigation of residual stress relaxation under cyclic load," Int. J. Fatigue, 2001.

[25] L. F. Impellizzeri, "Cumulative Damage Analysis in Structural Fatigue," Eff. Environ. Complex Load Hist. Fatigue Life, pp. 40–68, 1970.

[26] H. Jhansale and T. Topper, "Engineering Analysis of the Inelastic Stress Response of a Structural Metal Under Variable Cyclic Strains," in Cyclic Stress-Strain Behavior—Analysis, Experimentation, and Failure Prediction, 2009.

[27] R. Landgraf and R. Chernenkoff, "Residual Stress Effects on Fatigue of Surface Processed Steels," in Analytical and Experimental Methods for Residual Stress Effects in Fatigue, 2009.

[28] J. M. Potter, "The Effect of Load Interaction and Sequence on the Fatigue Behavior of Notched Coupons," in Cyclic Stress-Strain Behavior—Analysis, Experimentation, and Failure Prediction, 1973, pp. 109–132.

[29] K. I. M. Takanashi, K. Kamata, "Relaxation Behavior of Welding Residual Stresses by Fatigue Loading in Smooth Longitudinal Butt Welded Joints," Weld. World, vol. 44, 2000.

[30] S. Rao Valluri, "Some recent developments at 'GALCIT' concerning a theory of metal fatigue," Acta Metall., 1963.

[31] Q. Wang, X. Liu, Z. Yan, Z. Dong, and D. Yan, "On the mechanism of residual stresses relaxation in welded joints under cyclic loading," Int. J. Fatigue, 2017.

[32] O. S. Zaroog, A. Ali, B. B. Sahari, and R. Zahari, "Modeling of residual stress relaxation of fatigue in 2024-T351 aluminium alloy," Int. J. Fatigue, 2011.

[33] C. H. Lee, K. H. Chang, and V. N. Van Do, “Finite element modeling of residual stress relaxation in steel butt welds under cyclic loading,” Eng. Struct., 2015.

[34] A. A. Deshpande, D. W. J. Tanner, W. Sun, T. H. Hyde, and G. McCartney, “Combined butt joint welding and post weld heat treatment simulation using SYSWELD and ABAQUS,” Proc. Inst. Mech. Eng. Part L J. Mater. Des. Appl., 2011.

[35] D. Rosenthal, “The theory of moving sources of heat and its application to metal treatments,” Trans. ASME, vol. 68, pp. 849–866, 1946.

[36] J. Goldak, A. Chakravarti, and M. Bibby, “A new finite element model for welding heat sources,” Metall. Trans. B, 1984.

[37] L. E. Lindgren, “Finite element modeling and simulation of welding part 1: Increased complexity,” J. Therm. Stress., 2001.

[38] L. E. Lindgren, “Finite element modeling and simulation of welding. part 2: Improved material modeling,” J. Therm. Stress., 2001.

[39] L. E. Lindgren, “Finite element modeling and simulation of welding. Part 3: Efficiency and integration,” J. Therm. Stress., 2001.

[40] J. L. Chaboche and G. Rousselier, “On the plastic and viscoplastic constitutive equations-part I: Rules developed with internal variable concept,” J. Press. Vessel Technol. Trans. ASME, 1983.

[41] J. L. Chaboche and P. M. Lesne, “A NON-LINEAR CONTINUOUS FATIGUE DAMAGE MODEL,” Fatigue Fract. Eng. Mater. Struct., 1988.

[42] A. Laamouri, H. Sidhom, and C. Braham, “Evaluation of residual stress relaxation and its effect on fatigue strength of AISI 316L stainless steel ground surfaces: Experimental and numerical approaches,” Int. J. Fatigue, 2013.

[43] A. Mehmanparast, O. Adedipe, F. Brennan, and A. Chahardehi, “Welding sequence effects on residual stress distribution in offshore wind monopile structures,” Frat. ed Integrita Strutt., 2016.

[44] A. Mehmanparast, J. Taylor, F. Brennan, and I. Tavares, “Experimental investigation of mechanical and fracture properties of offshore wind monopile weldments: SLIC interlaboratory test results,” Fatigue Fract. Eng. Mater. Struct., 2018.

[45] A. Mehmanparast, F. Brennan, and I. Tavares, “Fatigue crack growth rates for offshore wind monopile weldments in air and seawater: SLIC inter-laboratory test results,” Mater. Des., 2017.

[46] J. Outinen, “Mechanical properties of structural steel at elevated temperatures and after cooling down,” in 10th International Conference - Fire and Materials 2007, 2007.

[47] L. Arany, S. Bhattacharya, J. Macdonald, and S. J. Hogan, “Design of monopiles for offshore wind turbines in 10 steps,” Soil Dyn. Earthq. Eng., 2017.